JOURNAL OF GEOPHYSICAL RESEARCH, VOL. 111, A11216, doi:10.1029/2005JA011092, 2006

Ballooning instability at the plasma sheet–lobe interface and its implications for polar arc formation

I. V. Golovchanskaya,[1] A. Kullen,[2] Y. P. Maltsev,[1,3] and H. Biernat[4]

Received 20 February 2005; revised 19 January 2006; accepted 8 August 2006; published 16 November 2006.

[1] Huang et al. (1987, 1989) reported hot filaments of plasma sheet origin filling the magnetospheric lobes during northward interplanetary magnetic field (IMF). On the other hand, cold plasma transients of presumably lobe origin are often observed in the plasma sheet. These features can be interpreted in terms of plasma exchange at the plasma sheet–lobe interface (PSLI) proceeding in a filamentary manner. We present a description of this process within ballooning destabilizing of the near-Earth curved segment of the PSLI. Although the basic ballooning instability condition is not typically met inside the plasma sheet, it is satisfied at this segment. The PSLI always separates the cold lobe population from the hot plasma sheet, thus providing a pressure gradient favorable for the instability; its near-Earth part has a nonnegligible magnetic curvature. A solution for the least stable ballooning harmonics is found, which satisfies the finite conductivity boundary condition in the ionosphere and the outgoing Alfvén wave condition at the tailward end of the near-Earth curved segment of the plasma sheet boundary. We show that this part of the PSLI may be a generator region launching filamentation. The background convection is imposed on the ballooning motions. The large-scale convection associated with southward IMF B_z suppresses hot filament progression into the lobes, while promoting penetration of lobe transients into the plasma sheet. However, during northward IMF, the convection favors at certain magnetic local times the extension of plasma sheet filaments into the lobes and their subsequent protrusion toward noon. This process is signified in the ionosphere by the occurrence of nightside originating polar arcs. Several polar arc events are shown that develop from the nightside oval boundary into the polar cap on timescales of approximately 10–15 min, consistent with the growth rates of the studied instability.

Citation: Golovchanskaya, I. V., A. Kullen, Y. P. Maltsev, and H. Biernat (2006), Ballooning instability at the plasma sheet–lobe interface and its implications for polar arc formation, *J. Geophys. Res.*, *111*, A11216, doi:10.1029/2005JA011092.

1. Introduction

1.1. Polar Arc Observations

[2] Since the first report of a large-scale transpolar arc connecting the dayside with the nightside auroral oval [*Frank et al.*, 1982], many different polar arc formations have been reported. Far from all are truly Sun-aligned, and not all reach the dayside oval. Although most transpolar arcs separate from the dawnside or duskside oval [*Chang et al.*, 1998], even nightside originating transpolar arcs may occur [*Craven et al.*, 1986]. The latter polar arc type is rather rare. In a recent statistical study by *Kullen et al.* [2002], covering 3 months of Polar UVI data, only 7 of 73 large-scale polar arcs were found to emerge as single arcs from the nightside and stretch toward noon (referred to as midnight arcs). In another six cases, nightside originating arcs are part of multiple arc events with three or more arcs filling the polar cap. A low occurrence rate of nightside originating arcs has been reported by *McEwen and Zhang* [2000] as well. They analyzed data from the meridian-scanning photometer Eureka, which has a much higher sensitivity than Polar UVI. It should be mentioned, however, that even those auroral arcs that develop at the dawn or dusk oval side, may involve a motion from the nightside to noon while separating from the oval side [*Kullen et al.*, 2002].

[3] It is commonly agreed on that large-scale polar arcs are genetically related to the plasma sheet or its boundary layer, as they have similar particle characteristics to those along the main oval [e.g., *Frank and Craven*, 1988; *Huang et al.*, 1989]. Most large-scale polar arcs are found to appear in a region of sunward convecting plasma [e.g., *Frank et al.*, 1986; *Cumnock et al.*, 2002].

[4] It is well known that the occurrence of polar arcs is connected to solar wind conditions. Polar arcs appear most commonly for large IMF magnitudes and high solar wind velocity [*Kullen et al.*, 2002]. They are a predominantly northward IMF phenomenon [*Frank et al.*, 1986; *Valladares et al.*, 1994], and their motion is controlled by the direction

[1]Polar Geophysical Institute, Apatity, Russia.
[2]Swedish Institute of Space Physics, Uppsala, Sweden.
[3]Deceased 3 June 2005.
[4]Space Research Institute, Austrian Academy of Sciences, Graz, Austria.

0148-0227/06/2005JA011092$09.00

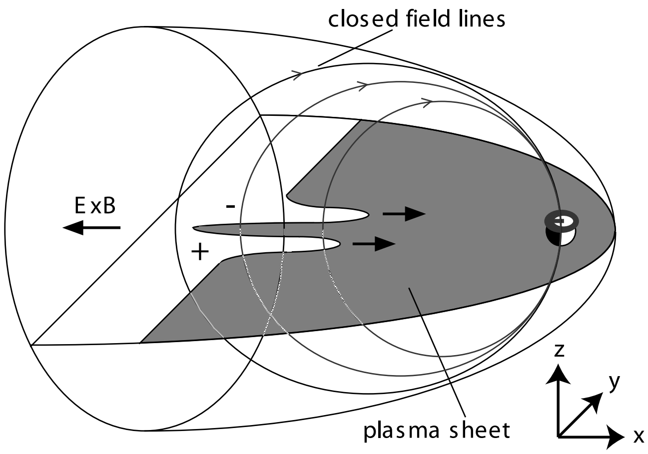

Figure 1. Interchange instability conditioned by the equatorial curvature of the short plasma sheet during substorm recovery, surrounded by closed magnetic tubes formed after an interplanetary magnetic field (IMF) north turn [*Rezhenov*, 1995].

of IMF B_y [*Valladares et al.*, 1994; *Huang et al.*, 1989; *Kullen et al.*, 2002]. In recent years, it has been suggested that sign changes in IMF B_z or B_y may trigger the evolution of transpolar arcs. *Newell et al.* [1997] and *Chang et al.* [1998] both suggested that an abrupt IMF sign change leads to a jump in the dayside reconnection site, causing a new region of open flux equatorward of the original polar cap boundary, the arc appearing on the closed field line bridge between the old and new polar cap region. As suggested by *Kullen* [2000] and confirmed in several MHD simulations [e.g., *Kullen and Janhunen*, 2004], the poleward motion and long lifetime of transpolar arcs can be explained by a large-scale tail reconfiguration after an IMF B_y sign change (a rotation of the tail twist) which causes a closed field line filament to move through the tail lobes and polar caps of both hemispheres.

[5] None of these models address the possibility of a nightside originating polar arc. A rather unknown model by *Rezhenov* [1995] explains the evolution of midnight arcs with an interchange instability occurring at the tailward end of the plasma sheet that leads to the development of a tongue (or tongues) of hot plasma moving tailward with the reverse motion on both sides (see Figure 1). His model requires a region of dipolarized closed field lines even tailward of the plasma sheet. This scenario may appear during substorm recovery after an IMF north turn, where newly closed magnetic tubes appear in a lower pressure region tailward of a short (not yet fully expanded) plasma sheet. *Rezhenov* [1995] predicts the arcs will form within 8–10 min on a highly contracted oval, while the oval regions adjacent to the arc retreat equatorward. An IMF north turn during the substorm explains the strong contraction of the polar cap boundary [*Kullen et al.*, 2002].

[6] These predictions fit well to the conditions found for midnight arcs (one single arc rising from the nightside oval to noon) in the work of *Kullen et al.* [2002]. The reported midnight arcs appear all at the end of substorm recovery, during which the oval has contracted considerably in connection with an IMF north turn. All midnight arcs start to develop from an extremely polewardly displaced bulge; their motion toward the noon part of the oval takes 10–20 min. While the arc grows toward noon, the poleward oval boundary retreats equatorward until the oval has reached its presubstorm size.

[7] Nightside originating arcs occurring outside substorm recovery do not fulfil the requirements for the interchange instability at the tailward plasma sheet boundary. In the work of *Kullen et al.* [2002] all nightside originating arcs that appear outside substorm recovery are parts of multiple arc events. These appear in general during quiet times with predominantly northward IMF, rather high IMF magnitude and solar wind speed. According to the T96 model [*Tsyganenko*, 1995], during northward IMF, the tailward extension of the closed field line region exceeds 160 R_E for both strongly and weakly northward IMF (see Figure 2, left and middle plots). More important is that the plasma

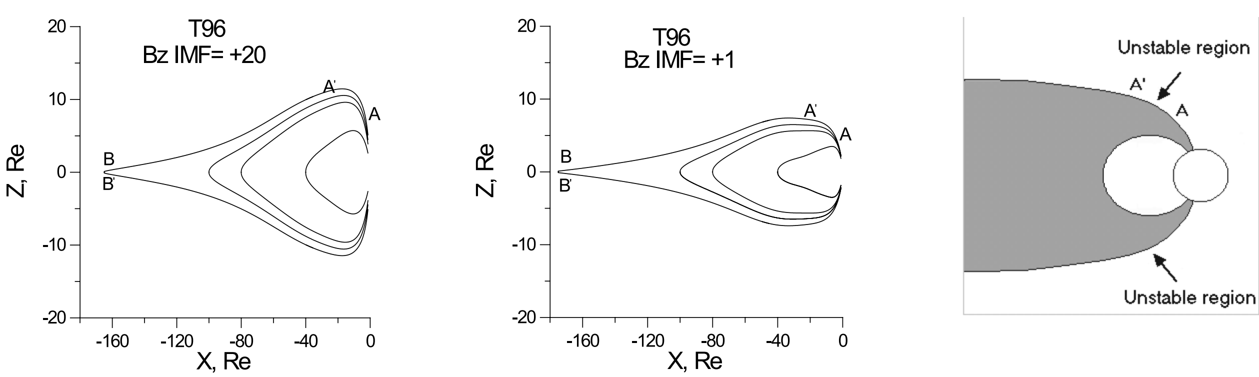

Figure 2. Statistical magnetic configurations for (left) strong and (middle) weak northward IMF (given in nT) according to the T96 model, for y = 0 and zero dipole tilt. Note an increase in the near-Earth curvature of the boundary plasma sheet with increasing northward IMF B_z. (right) An idealized configuration which is adopted in the calculations: The boundary field line is broken into two sections; one (AA′) is basically circular, and the other (downtail of A′) abutted to this partial circle is basically straight. The ballooning instability occurs in the circular section, and the straight section is simply dragged along.

population remains the same earthward and tailward of the last closed field line during these conditions [*Song et al.*, 1999; *Kullen and Janhunen*, 2004]. The strong earthward plasma pressure gradient, necessary for a ballooning growth, does not form.

[8] In this study a modification of the ballooning mechanism is proposed that may explain nightside originating polar arcs, which are not related to substorm recovery. The modification considers the near-Earth curved segment of boundary magnetic field lines to be responsible for the ballooning destabilizing and motion of plasma filaments into the lobes. Such plasma filaments have been observed during northward IMF conditions [*Huang et al.*, 1987, 1989].

1.2. Ballooning Mode Formulations for the Earth's Magnetosphere

[9] For the last two decades the ballooning modes, for which rigorous mathematical description based on the energy principle was given in the work of *Hameiri et al.* [1991] and references therein, have been repeatedly invoked for interpretation of various magnetospheric phenomena. *Lakhina et al.* [1990] presented an eigenmode structure analysis of the ballooning perturbations in the far tail in the presence of sheared field-aligned plasma flow, the latter considered to be a source of the free energy. The authors found that ballooning destabilizing is possible if the flow pressure gradient is large and applied their results for the interpretation of the large-scale magnetic structures with alternating sign of the B_z component observed in the distant tail by ISEE 3. *Roux et al.* [1991] considered the ballooning instability in the equatorial near-Earth tail as a possible trigger of substorm expansion. Their consideration was mostly based on the ballooning formulation of *Miura et al.* [1989], who extended the ideal MHD ballooning theory to the case where a cross-tail ion drift is included, aiming to explain Pc 5 pulsations. Later, the possibility that the ballooning instability can be a substorm trigger was alternatively discarded and rehabilitated. *Lee and Wolf* [1992] demonstrated from the energy principle that typical magnetotail configurations are stable to both compressible symmetric ideal MHD ballooning and interchange modes, the perfectly conductive ionosphere was inferred. In the analysis of *Lee and Wolf* [1992], the free energy was considered to be stored in the radial pressure gradient of the equatorial magnetotail. In the studies by *Ivanov et al.* [1992], *Liu* [1996], and *Golovchanskaya and Maltsev* [2003] it was pointed out that the configurations with longitudinal asymmetry may be ballooning/interchange unstable, the free energy being provided by an external source through maintaining the directional displacement between the pressure gradient and magnetic curvature vectors. *Liu* [1996] argued that the instability of this kind may set up the general inhomogeneous background in which the disruption of the cross-tail current and substorm initiation occur. Furthermore, *Liu* [1997] demonstrated that the conclusion of *Lee and Wolf* [1992] that the Earth's magnetotail is balloon stable, stems from the suggestion of a standing ballooning structure in their formulation, and is not relevant if one considers the ballooning perturbations as free propagating waves noninfluenced by the boundaries. In the local analysis that he performed, two solutions for the ballooning modes were found. One corresponds to the Alfvén-type ballooning mode which transfers into the Alfvén wave if the plasma parameter $\beta = 2\mu_0 p/B^2$ tends to zero. The necessary condition for this mode destabilizing is

$$k_p - \gamma(k_B + k_c) > 0, \qquad (1)$$

where k_p and k_B are the reversed scales of equilibrium pressure p and magnetic strength B inhomogeneity toward the curvature center, respectively, k_c the reversed curvature radius, γ the adiabatic exponent. The other solution obtained by *Liu* [1997] describes the slow magnetosonic type ballooning mode, for which the parallel component of velocity perturbation is essential. This mode is shown to be unstable in a high-β plasma with a pressure gradient of any magnitude directed toward the curvature center. The instability growth times of $\sim$1 min can be related to the explosive growth phase of a substorm in the magnetosphere [*Liu*, 1997].

[10] Recently, the local analysis of *Liu* [1997] has been generalized for the ballooning perturbations with a component of the wave vector along the magnetic tension force [*Golovchanskaya and Maltsev*, 2005]. The obtained solution in the stable case describes the ballooning waves, which group velocity has a component in the positive/negative azimuthal direction. The results were applied for the interpretation of plasma sheet flapping waves observed by Cluster.

[11] Criterion (1) was tested for the equatorial magnetotail by *Ohtani and Tamao* [1993] on the basis of spacecraft observations. They demonstrated in statistics that it almost never holds inside the plasma sheet (the substorm recovery conditions considered by *Rezhenov* [1995] may be an exception). At the same time, those authors pointed out that condition (1) is presumably satisfied in the boundary region of the plasma sheet (the near-Earth curved segment AA′ of the last closed magnetic field line shown in Figure 2). This curvilinear site always separates lower pressure plasma of the lobe from hotter plasma sheet population, thus providing a pressure gradient in favour of the instability. The overall configuration is heavy-upon-light liquid type in the presence of gravity. In case of the magnetosphere, the role of the gravity is taken by the curved magnetic field, acting through the magnetic tension force on the hot plasma. Ballooning destabilizing of this region will lead to filamentary extensions of the plasma sheet into the lobes and the lobes into the plasma sheet. Around the segment AA′ k_p is large, k_B is negative, and k_c is relatively small. To make estimates, we take the characteristic curvature radius $R_c \sim 20\ R_E$ ($k_c \sim 0.05\ R_E^{-1}$), R_E being the Earth's radius, the scale of the e fold pressure increase toward the curvature center by an order of magnitude smaller ($k_p \sim 0.5\ R_E^{-1}$) and the plasma parameter $\beta \sim 0.5$. Then from the force-balance condition written for the static equilibrium as

$$\beta/2\ k_P + k_B - k_c = 0 \qquad (2)$$

we have $k_B \sim -0.075\ R_E^{-1}$. One can see that with these quantities condition (1) is well satisfied. Inequality (1) is not, however, a sufficient condition for the ballooning instability, for it does not include the stabilising term proceeding from the field line bending.

[12] The purpose of the present paper is to assure that the near-Earth curvilinear region of the PSLI is ballooning unstable by performing analysis of the standing structure formed by Alfvén type ballooning perturbations at AA′ segment, nonperfectly conductive ionosphere supposed, and consider possible implications for nightside polar arc formation. In doing that, we will impose the following boundary condition at the ionospheric foot of magnetic field tube (point A) [*Maltsev*, 1977; *Glassmeier*, 1983]

$$\frac{\partial}{\partial s}\varphi|_A = i\mu_0\omega\Sigma_P\varphi. \quad (3)$$

Equation (3) states that at the ionospheric level the field-aligned currents in the ballooning perturbations must be closed by the ionospheric currents. In equation (3), ω is the frequency of the perturbation, φ the transverse displacement of the magnetic field line multiplied by the metric factor $\sqrt{B}$, Σ_P the height-integrated Pedersen conductivity of the ionosphere, μ_0 the magnetic permeability of vacuum, s the coordinate along the magnetic field line, such that s = 0 at the ionospheric end of the tube.

[13] At the point A′ we will impose a condition of the outgoing Alfvén wave

$$\frac{\partial\varphi}{\partial s}|_A = -i\omega\mu_0\Sigma_W\varphi, \quad (4)$$

where $\Sigma_W = 1/(\mu_0 V_A)$ is the wave conductivity, $V_A \sim 10^3$ km/s is the Alfvén velocity. Condition (4) implies that the perturbed field-aligned currents tailward of A′ close via the Alfvén front going to infinity (Figure 2, right plot). As is further shown, the growth time of the instability under study is at least by an order of magnitude shorter than the forth-back transit time of an Alfvén wave travelling along the last closed magnetic field line (for the left and middle configurations in Figure 2 this time exceeds 1 hour). We will also argue that at the nonlinear stage the instability results in hot tube detachment from the plasma sheet and progressing toward the dayside cusp. It will be shown that the foot of a tube travels a distance comparable to the dimension of the polar cap in the time required for an Alfvén wave to reach the opposite ionosphere and come back. All this justifies condition (4), which presupposes that for the considered geometry there is no Alfvén-wave communication with the opposite ionosphere. Further, we will adopt $\Sigma_W \sim 0.8$ S for the boundary plasma sheet and $\Sigma_P \sim 2$ S for its ionospheric footprint.

[14] To our knowledge, only few of so far proposed ballooning formulations [*Hameiri et al.*, 1991; *Ivanov et al.*, 1992] address the case of nonperfectly conducting boundaries. Not only is the finitely conductive ionosphere physically more appropriate (for night hours Σ_P does not typically exceed a few S), more important is that the condition of a perfectly conductive ionosphere suggests zero ballooning perturbations at the boundaries, so that the least stable zeroth ballooning harmonics in the standing structure that forms at the curvilinear site appears to be dropped.

[15] In the present study we focus on the near-Earth curved section of the plasma sheet–lobe interface AA′ (Figure 2). In principle, the equatorial curved site of the last closed magnetic field tube BB′ (Figure 2) could also become ballooning unstable. However, as mentioned above, there is no indication of strong pressure gradients necessary for a ballooning growth around this site, as the plasma sheet continues tailward of the last closed field line [*Song et al.*, 1999; *Kullen and Janhunen*, 2004]. The magnetic field is singular just tailward of BB′, its integral curvature being uncertain.

[16] Further, in section 2 we will consider the ballooning instability conditioned by the near-Earth curvature of the boundary plasma sheet in more detail. The dispersion relation for the instability and estimates for the linear growth rates are given in section 2.1; nonlinear stage and influence of the background convection are considered in section 2.2. Samples of midnight and multiple arc events, which we suppose to be ionospheric signatures of the ballooning instability, are illustrated and described in section 3. The major results are discussed in section 4.

2. Ballooning Instability Related to the Near-Earth Curvature of the Plasma Sheet–Lobe Interface

2.1. Dispersion Relation

[17] Previously, the dispersion relation for the ideal MHD Alfvén type ballooning mode was obtained in the local approximation by *Ohtani and Tamao* [1993] (in the present paper we do not address the ballooning mode related to the field-aligned velocity perturbations [*Liu*, 1997]). It has the form

$$\omega^2 = V_A^2 k_\|^2 - \omega_g^2, \quad (5)$$

where $k_\|$ is the field-aligned component of the wave vector and ω_g is given by

$$\omega_g^2 = \frac{\beta V_A^2}{1+\frac{\gamma\beta}{2}} k_c \left[k_p - \gamma(k_b + k_c)\right]. \quad (6)$$

[18] As was mentioned above and as follows from equation (6), ω_g^2 is positive for the adopted values of the equilibrium parameters, with $\omega_g \sim 0.015\ s^{-1}$.

[19] In deriving equation (5) it was supposed that the perpendicular component of the wave vector of the perturbation is directed along the y_{GSM}-axis and greatly exceeds any other scale size of the problem. In such a case, if we roughly take that the equilibrium characteristics (V_A, k_c, etc.) do not change significantly along the curvilinear segment of the boundary magnetic field line (Figure 2, right plot), solution (5) can be referred to the section AA′ as a whole.

[20] The boundary conditions (3), (4) yield one more relation between the frequency ω and field-aligned wave number $k_\|$ of the perturbation

$$\left(k_\|^2 + \omega^2\mu_0^2\Sigma_P\Sigma_W\right)\mathrm{tg}\ k_\| a = -i\ \omega\mu_0(\Sigma_P + \Sigma_W)k_\|, \quad (7)$$

where the length of the section AA′ is denoted as a ($a \sim 20\ R_E$).

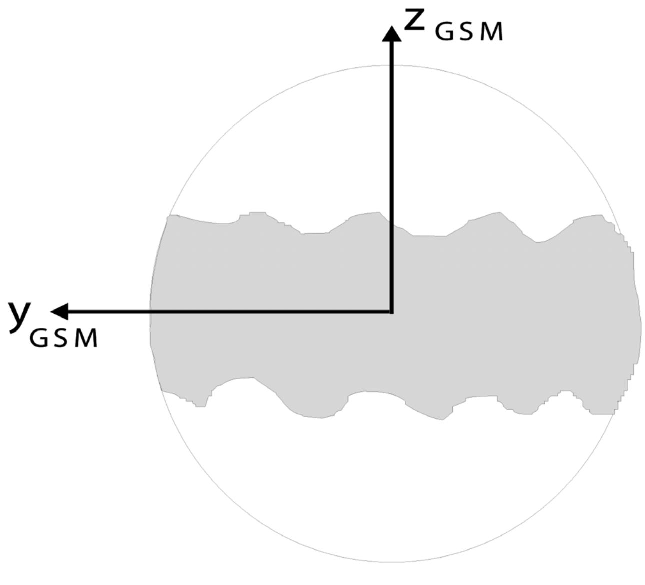

Figure 3. Undulation of the plasma sheet–lobe interface at the linear stage of the ballooning instability conditioned by the near-Earth magnetic curvature.

[21] In the ballooning structure determined by (5) and (7) the most promising for destabilizing is the zeroth harmonics ($k_{\|}\ a \ll 1$), for it is for this harmonics that the stabilizing term $V_A^2\ k_{\|}^2$ proceeding from magnetic bending is the smallest. In the limit $k_{\|}\ a \ll 1$, equation (7) takes the form

$$\left(k_{\|}^2 + \omega^2 \mu_0^2 \Sigma_P \Sigma_W\right) a = -i\ \omega \mu_0 (\Sigma_P + \Sigma_W). \quad (8)$$

Substituting $k_{\|}$ from (5) into (8), we have

$$\omega^2 \left(1 + \mu_0^2 V_A^2 \Sigma_P \Sigma_W\right) a + i\ \omega \mu_0 V_A^2 (\Sigma_P + \Sigma_W) + \omega_g^2 a = 0. \quad (9)$$

We note that in equation (9) both inertial and bending terms are preserved. Considering that ω_g^2 is positive, both solutions of the quadratic equation (9) are purely imaginary, meaning aperiodic regime without oscillations. The unstable solution is given by

$$\omega = -\frac{iV_A}{2a} + \left[-\left(\frac{V_A}{2a}\right)^2 - \frac{\omega_g^2}{\left(1 + \frac{\Sigma_p}{\Sigma_W}\right)} \right]^{1/2}. \quad (10)$$

It can be seen that the unstable mode (10) vanishes if $\Sigma_P \to \infty$ or $\omega_g \to 0$. For the adopted values of the parameters, ω can be estimated as $\sim 0.5 \cdot 10^{-2}\ s^{-1}$, which corresponds to the instability growth times of 3–4 min. For other characteristic parameters for the equilibrium, the growth rate varies in the range 10^{-2}–$10^{-3}\ s^{-1}$.

[22] The mode revealed has both ballooning and interchange sense. Formally, $k_{\|}$, though small, is nonzero for it, which is a feature of ballooning perturbations. On the other hand, solution (10) describes the case, when a magnetic tube departs from the equilibrium position without essential deformations associated with the Alfvén propagation, and this makes it similar to the interchange mode. Figure 3 sketches the undulation of the PSLI at the linear stage of the ballooning instability conditioned by the near-Earth magnetic curvature.

[23] We have found that the growth time of the instability under study is as short as a few minutes. This suggests that most of the time it evolves in the nonlinear regime, which will further be considered.

2.2. Nonlinear Stage and Influence of the Background Convection

[24] At the nonlinear stage, plasma sheet extensions into the lobes can either be filaments, that is, hot tubes detached from the plasma sheet and making up roads along convection streamlines, or solid sheets in the XZ plane. If we carefully look at the snapshots or images of extension footprints in the ionosphere (Figure 4), we will see that they are never solid or smooth but always made up of smaller-scale features of increased luminosity. This observation infers a filamentary manner of the extension (Figure 5, top) rather than the solid one (Figure 5, bottom). The tubes detached from the plasma sheet are still curved in the near-Earth region and filled with hot plasma. Then they tend to continue their motion away from the plasma sheet, as the final cause of this motion is a charge separation due to a divergence of energetic ion drift current in a curved/inhomogeneous magnetic field. We note that a similar evolution of the ballooning instability in a laboratory plasma was observed by *Alfvén* [1981].

[25] Let us find the footprint velocity v_{hi} of a hot filament with a circular cross section in the reference frame of the background convection. Previously, treatments of transient motions were performed by *Lyatsky and Maltsev* [1984] and *Pontius and Wolf* [1990] for the Earth's inner plasma sheet and by *Pontius and Hill* [1989] for Iogenic plasma.

[26] The divergence of the gradient-curvature current $\mathbf{j}_\perp$ is given by

$$\mathrm{div}\ \mathbf{j}_\perp = \frac{1}{B^2}\mathrm{div}[\mathbf{B} \times \nabla p] + \nabla\left(\frac{1}{B^2}\right) \cdot [\mathbf{B} \times \nabla p]. \quad (11)$$

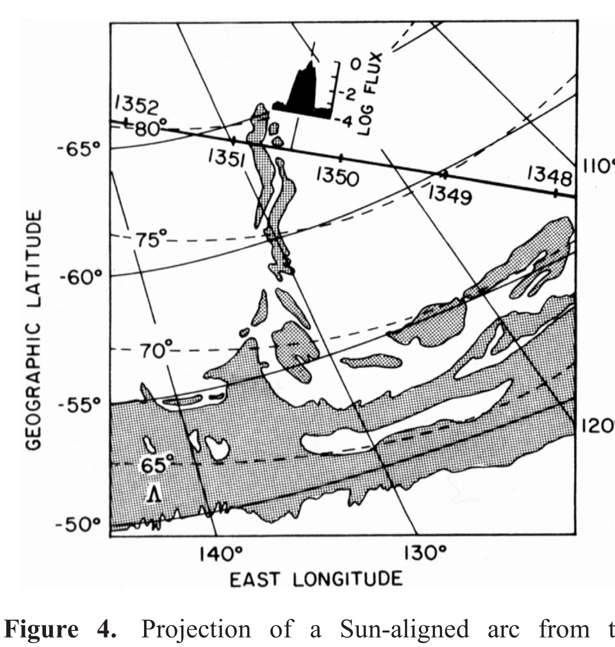

Figure 4. Projection of a Sun-aligned arc from the nightside auroral oval into the polar cap [from *Hoffman et al.*, 1985].

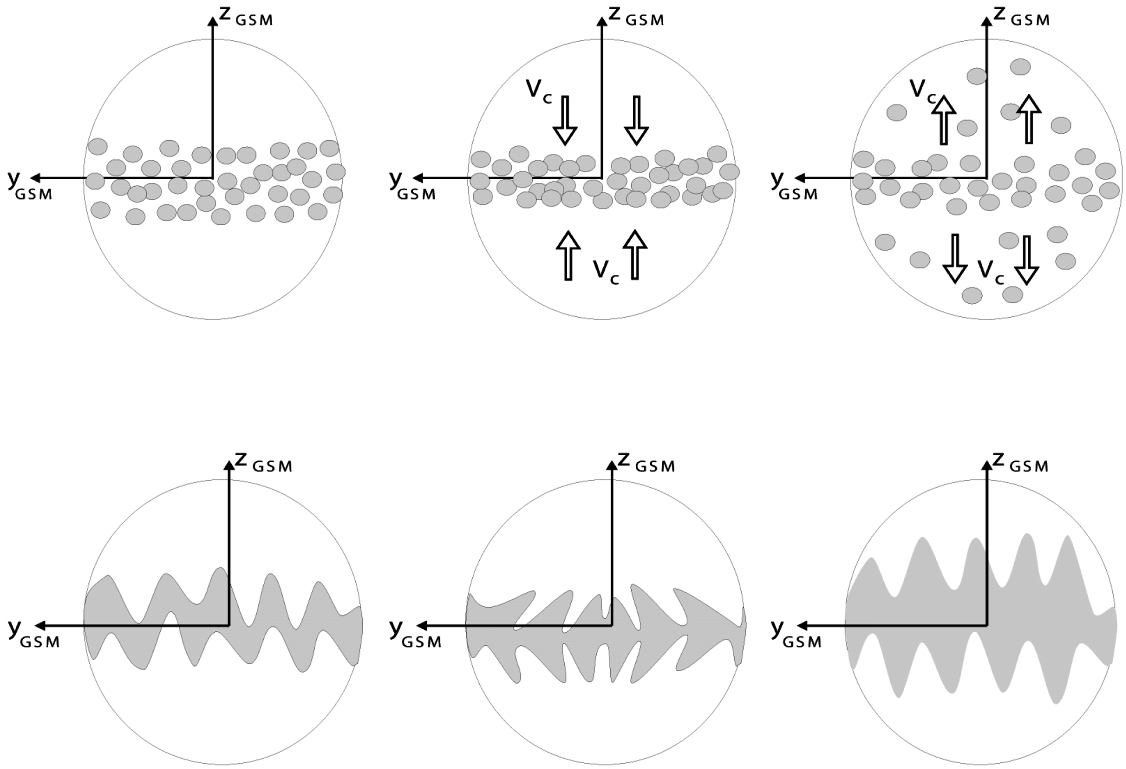

Figure 5. Schematic of plasma sheet transformations at the nonlinear stage of the ballooning instability for (top) intermittent and (bottom) continuous plasma exchange at the PSLI (left) in the absence of background convection, (middle) for the magnetospheric convection during southward IMF, and (right) for the magnetospheric convection during northward IMF.

Noticing that div $[\mathbf{B} \times \nabla \mathrm{p}] = \nabla \mathrm{p} \cdot \mathrm{rot}\, \mathbf{B} - \mathbf{B} \cdot \mathrm{rot}\, \nabla \mathrm{p}$, both terms in the RHS being zero, we have

$$\mathrm{div}\, \mathbf{j}_\perp = -\mathbf{B}\left[\nabla\left(\frac{1}{B^2}\right) \times \nabla \mathrm{p}\right] = \mathbf{B}\left[\frac{\nabla B^2}{B^4} \times \nabla \mathrm{p}\right]. \qquad (12)$$

Using the force balance equation $\nabla \mathrm{B}^2 = -2\, \mu_0\, \nabla \mathrm{p} + 2\, \mathbf{k}_\mathrm{c}\, \mathrm{B}^2$, we can rewrite (12) as

$$\mathrm{div}\, \mathbf{j}_\perp = \frac{2}{B} \mathbf{e}_\mathrm{b}[\mathbf{k}_\mathrm{c} \times \nabla \mathrm{p}], \qquad (13)$$

where $\mathbf{e}_\mathrm{b}$ is the unit vector along the magnetic field. Then the field-aligned current $\mathrm{j}_\parallel$ in the northern ionosphere is

$$\mathrm{j}_\parallel = -\mathrm{B}_\mathrm{i} \int \frac{\mathrm{div}\, \mathrm{j}_\perp}{B} ds = -\mathrm{B}_\mathrm{i} \int \frac{2}{B^2} \mathbf{e}_\mathrm{b}[\mathbf{k}_\mathrm{c} \times \nabla \mathrm{p}] ds, \qquad (14)$$

where B_i is the magnetic field at the ionospheric level. It is seen that the integration in (14) extends only over the near-Earth curvilinear segment of the hot tube, for which $\mathbf{k}_\mathrm{c} \neq 0$. It is also seen that the field-aligned current is positive (into the ionosphere) at the dusk side of the hot filament and negative (out of the ionosphere) at its dawn side.

[27] Now we use the current continuity equation

$$-\mathrm{B}_\mathrm{i} \int \frac{2}{B^2} \mathbf{e}_\mathrm{b}[\mathbf{k}_\mathrm{c} \times \nabla \mathrm{p}] ds = (\Sigma_\mathrm{P} + \Sigma_W) \mathrm{div}\, \mathbf{E}, \qquad (15)$$

where **E** is the polarization electric field to be found. We will consider the difference in pressure between the hot tube and the background to be a step function, the pressure of the lobe plasma taken zero. Then the solution of (15) is the electric field **E**, which is uniform and directed from dusk to dawn inside the filament and subsides as a 2D dipole field from its boundary outward [e.g., *Pontius and Wolf*, 1990]. Taking into account that the tangential component of the electric field must be continuous at the filament boundary and that the radial component suffers a jump equal to the double value of the electric field inside the filament, we can find the value of this latter field

$$E = -\frac{B_i^{1/2} p}{(\Sigma_P + \Sigma_W)} \int \frac{k_c}{B^{3/2}} ds, \qquad (16)$$

where it has been suggested that $|\nabla_\perp p| = (B/B_i)^{1/2}\, |\nabla_{\perp i} p|$. Correspondingly, the footprint velocity of a hot filament $v_{hi} = \frac{E}{B_i}$ can be written as

$$v_{hi} = -\frac{p}{(\Sigma_P + \Sigma_W) B_i^{1/2}} \int \frac{k_c}{B^{3/2}} ds \qquad (17)$$

in which the minus sign indicates that the motion is outward from the curvature center. It can be shown that the velocity v_{hi} ranges from 100 m/s to a few km/s, depending on which parameters are chosen. Taking the same quantities as for the estimation of ω from (10), we have $v_{hi} \approx 400$ m/s. Then the time required for the tube footprint to travel a distance equal to the size of the polar cap (~2000 km) is about 1.5 hour. This is comparable to the forth-back travel time of emitted Alfvén wave, thus making the above condition (4) plausible.

[28] We also note that for the real PSLI configurations (Figure 2, left and middle plots), the integrand in the RHS of (17) quickly subsides tailward of A′ (not considering the section BB′ for the reasons given above). This justifies the idealised model (Figure 2, right plot) that we have used in our calculations.

[29] It is interesting to compare the estimation for v_{hi} with the observed rate of a Sun-aligned arc protrusion into the polar cap. The event of such an extension shown in Figure 4 has been carefully examined by *Hoffman et al.* [1985]. During this event, a Sun-aligned arc originating in the near-Earth boundary plasma sheet, protruded from the nightside auroral oval well into a true polar cap. The latter was confirmed by polar rain precipitation and antisunward convection (IMF B_z near zero) from both sides of the arc. The velocity v_c of the background antisunward convection was in average 300 m/s. Inside the arc the sunward convection velocity amounted to 850 m/s. Thus we have v_{hi} of ~1 km/s for this case, which is consistent with the above estimates. Sunward velocities of the same order inside Sun-aligned arcs have been reported by *Valladares and Carlson* [1991].

[30] Another point worth mentioning about this event is that along with hot plasma portions going to the polar cap, one can clearly see cold plasma features entering the auroral oval and getting more latitudinally aligned, presumably owing to the background convection in the auroral oval. These can signify a reverse supply of lobe magnetic tubes into the plasma sheet.

[31] In general, at the nonlinear state of the instability evolution, we should expect plasma sheet dissolution into hot filaments, alternating with colder plasma features. The overall picture is given in Figure 5. The top plots refer to the case when the plasma exchange between the lobes and the plasma sheet is intermittent, whereas the lower row plots sketch a continuous process. The left column in Figure 5 corresponds to the absence of the background convection. If the lobe convection is associated with the southward IMF B_z and has a velocity v_c in excess of the hot filament velocity v_h, the filaments are not capable to exit from the plasma sheet. The plasma sheet is thinning (Figure 5, middle column). In opposite, during northward IMF, the magnetospheric convection (at certain MLTs) favours the extension of plasma sheet filaments into the lobes. As a result, the plasma sheet is swelling out (Figure 5, right column).

[32] In Figure 5 the background convection is assumed to be uniform. In reality, the sunward convection under northward IMF does not appear on the entire polar cap region, but in several Sun-aligned channels (this point will be addressed in more detail in section 4). Along these channels the extensions into the lobe may form, such that the plasma sheet filamentation resembles the schematic by *Huang et al.* [1989], (see section 4). Sunward convection channels appear typically during northward IMF, when multiple convection cells cover the polar cap. Their occurrence and shape is strongly dependent on IMF B_y and B_z [e.g., *Weimer*, 1995], which explains the IMF dependent motion of these arcs. A nice example of a transpolar arc moving over the polar cap and the connected change in the large-scale convection pattern is shown in the work of *Cumnock et al.* [2002]. For multiple arcs such conjunction observations are still missing.

[33] To complete this section we note that the density of the upward field-aligned current at the edge of a hot filament given by formula (14) exceeds the value of $\sim 10^{-6}$ A/m^2 for the scales in the y_{GSM} direction smaller than 50 km (when reduced to the ionosphere). This current density is sufficient to produce the field-aligned electron acceleration into the ionosphere and discrete arc formation. On larger transverse scales one should expect diffuse precipitation in association with the hot filaments detached from the plasma sheet.

3. Ionospheric Signatures of the PSLI Ballooning Instability

[34] Figures 6a and 6b contain Polar UVI images of two types of polar arcs, which we mean to relate to the ballooning instability considered in the previous section. The variations of solar wind parameters during these arc events are also presented. The images are produced with the integration period of 36 s. The spatial resolution of the imager is 50 × 50 km. The gray scale (shown at the bottom of Figure 6) is the same for all plots and extends from 0.2 to 20 photon cm^{-2} s^{-1}. The time resolution between the plots in Figures 6a and 6b is 12 min. For a comparison with the solar wind conditions we have used 5-min averaged measurements of the ACE satellite (located ~220 R_E sunward of the Earth). The data are shifted in time to take the propagation to the Earth's magnetopause into account (for more detail, see *Kullen et al.* [2002]).

[35] Figure 6a illustrates a time evolution of a clear midnight arc appearing at the end of a substorm recovery that starts at very high latitudes from a polewardly displaced bulge at the nightside oval boundary and moves toward noon. While stretching sunward, the adjacent oval regions move equatorward. IMF B_z was steadily northward (~4 nT) from 2000 UT to 2200 UT, followed by a small southward excursion at 2205 UT and a larger one at about 2230 UT. Starting from 2130 UT, IMF B_y was steadily positive (Figure 6, top plot). The solar wind velocity was moderately high (~550 km/s).

[36] Figure 6b refers to a multiple arc event, where the polar cap fills with many arcs within a short time span in a rather disordered manner. Generally, during such events the first arcs may separate from the dawn or dusk oval sides, the following arcs appear gradually inside the polar cap. Several of these involve a noonward motion. During the multiple arc event, as well as in the previous hour, IMF B_z was steadily positive (~5 nT), IMF B_y changed its sign frequently, and the solar wind velocity was close to the average value (~400 km/s). It was previously mentioned by *Kullen et al.* [2002] that the arcs of this type do not have any obvious external trigger. The only common solar wind conditions for multiple arcs are northward IMF 1–2 hours before the arcs start to appear, and an increased anti-epsilon parameter. This is the case for the event presented.

4. Discussion

[37] Among five types of large-scale polar arcs, the commonly observed oval-aligned and moving arcs have

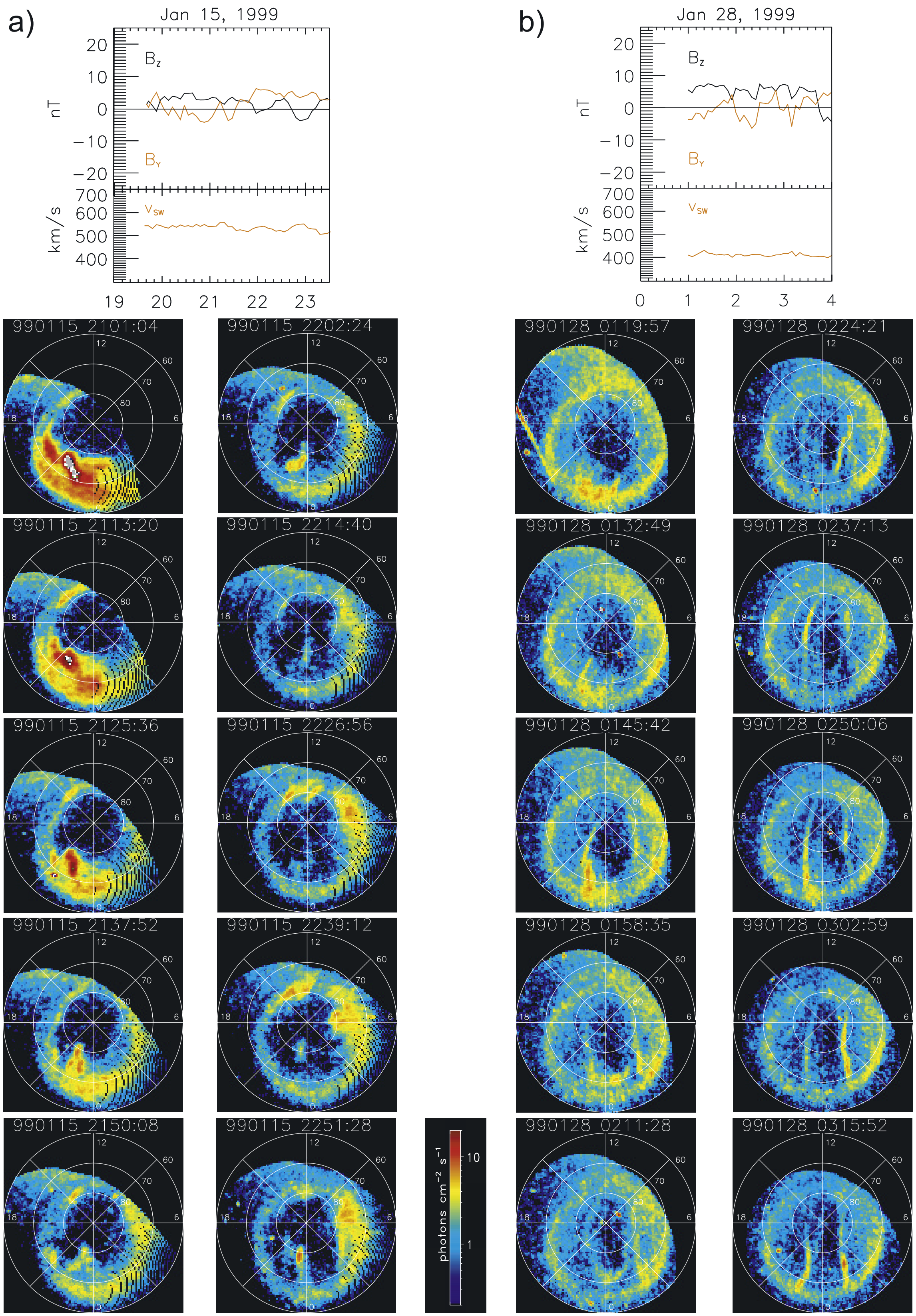

Figure 6. ACE solar wind data and Polar UVI plots of (a) a midnight arc and (b) a multiple arc event. The solar wind data are given in UT and have been corrected for the propagation time of 42.96 min (Figure 6a) and 59.84 min (Figure 6b).

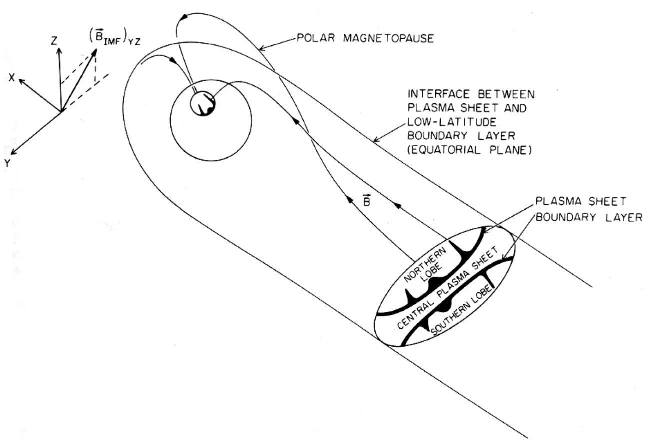

Figure 7. Extension of plasma sheet filaments into the lobes during northward IMF, as observed by *Huang et al.* [1987, 1989].

been reasonably explained in terms of IMF B_y induced tail twist [*Kullen et al.*, 2002]. Both arc types have been studied extensively. They typically appear on closed field lines and map to the plasma sheet [e.g., *Chang et al.*, 1998]. Oval-aligned arcs, even those that are clearly separated from the oval side, appear during constantly northward IMF on the dawn (dusk) oval side for negative (positive) IMF B_y. The motion across the entire polar cap toward the opposite side of the oval of moving arcs is triggered by IMF B_y sign change [*Cumnock et al.*, 2002].

[38] Arcs originating from the nightside (single midnight arcs and nightside originating arcs during multiple arc events) typically erupt out of auroral oval regions that are brighter than the surrounding regions, and rapidly progress into the polar cap. These features can be most easily interpreted as a result of boundary plasma sheet destabilizing. The very idea of an instability that could launch plasma sheet filaments into the lobes dates back to *Huang et al.* [1989] and is sketched in Figure 7 taken from their paper. In the present study we give a mathematical description of their hypothesis within ballooning instability scenario.

[39] As mentioned above, the ballooning instability does not work inside the plasma sheet. Sharp earthward (generally toward the curvature center) pressure gradients, needed for instability growth (see criterion (1)), typically do not form there. *Rezhenov* [1995] argues that under extraordinary conditions this still may be the case. He addresses substorm recovery, when a strongly dipolarized plasma sheet is surrounded by newly formed (after IMF north turn) closed magnetic field lines with a plasma of lower pressure (see Figure 1). Such conditions are obviously relevant for midnight arcs (see example in Figure 6a). We should keep in mind, however, that the filamentation in the Rezhenov model proceeds entirely on the closed field lines. The hot filaments do not enter the true polar cap and, consequently, cannot be influenced by the polar cap convection. As reported by *Kullen et al.* [2002], multiple arc events are not related to substorm recovery. This means that another ballooning modification should be invoked for their interpretation. In the present study we consider the near-Earth curvilinear segment of the PSLI (AA′ in Figure 2) and show that this site is ballooning unstable.

[40] It should be emphasized that the motion of the ballooning structures at the nonlinear stage is governed not only by their own polarization fields but also by the large-scale electric field. Therefore the progression of hot filaments into the lobes (as well as of lobe features into the plasma sheet) is strongly controlled by IMF clock angle and solar wind velocity via a corresponding pattern of magnetospheric convection. A schematic of the high-latitude flow pattern for rather strong northward IMF and different IMF B_y directions is given in Figure 8 taken from *Lassen* [1979]. It gives us a hint where hot filaments exit into the polar cap and subsequent protrusions toward noon are most probable.

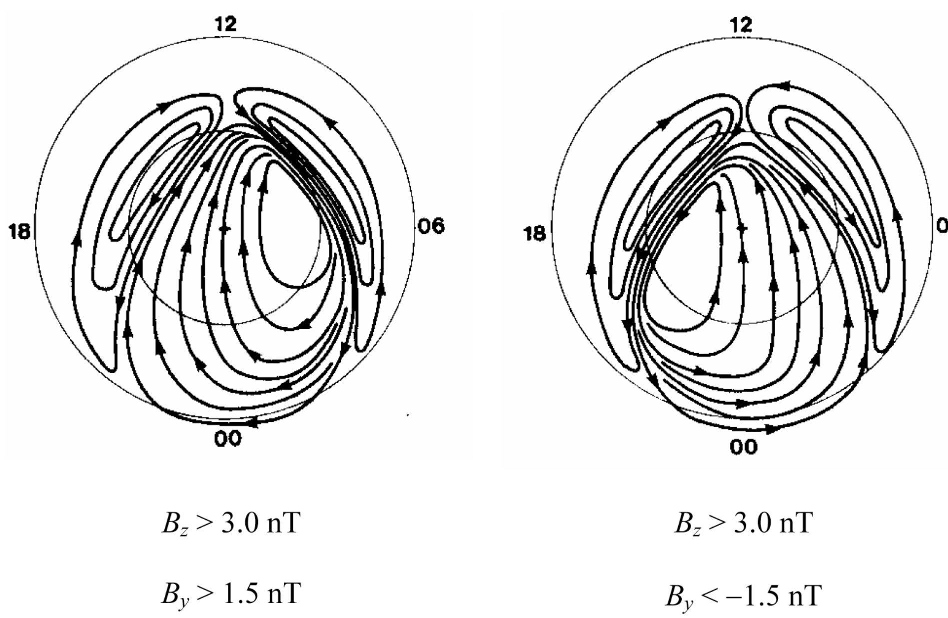

Figure 8. Schematic high-latitude convection pattern for strong northward IMF B_z and (a) duskward and (b) dawnward IMF B_y according to *Crooker* [1979] [see also *Lassen*, 1979].

Namely, if associated with the proposed mechanism, the multiple polar arcs in the Northern Hemisphere should be expected more frequently toward dusk from the noon-midnight meridian for positive IMF B_y and toward dawn from this meridian for negative IMF B_y. This is the case at least for the first clearly visible arc in the multiple arc cases reported by *Kullen et al.* [2002].

[41] We cannot exclude the possibility that even midnight arcs may result from PSLI ballooning destabilizing. Starting from onset, expanding substorm activity can reach the lobes, heating magnetic tubes in the boundary plasma sheet. This intensifies the ballooning process at the PSLI by increasing the lobe-to-plasma sheet pressure gradient (formally β in (6) increases). If by this time a favorable convection pattern, like that in Figure 8, has already formed (and this must be the case, for we refer to the late recovery phase) the hot extensions will proceed to the lobes. In the Northern Hemisphere, the midnight arcs should occur in the premidnight hours for IMF $B_y > 0$ and in the postmidnight hours for IMF $B_y < 0$. Generally, they should be more frequent in the premidnight hours, considering substorm activity peak in this MLT sector. With few exceptions all the above predictions about the IMF B_y dependence of midnight and multiple arcs are confirmed statistically by *Kullen et al.* [2002, Table 1].

[42] We should point out, however, that the flow pattern shown in Figure 8 is strongly idealized. The convection inferred from electric field observations in the polar cap is much more complicated, sometimes with several convection cells and only one or two rather narrow channels of sunward convection in between [e.g., *Weimer*, 1995]. This implies more complicated polar arc manifestations, such as the fast motion and merging of different polar arcs, as shown in the multiple polar arc event by *Newell et al.* [1997].

[43] The present study has been concentrated on the evolution of hot filaments generated by the ballooning instability at the PSLI with implications for polar cap arcs. At the same time, the ballooning mechanism suggests a simultaneous formation of cold transients penetrating into the plasma sheet. Such features have been reported in a number of studies [e.g., *Pontius and Wolf*, 1990; *Angelopoulos et al.*, 1992; *Sergeev et al.*, 2000]. North-south-aligned filamentary structures of a thick plasma sheet during strongly northward IMF have been found by *Petrukovich et al.* [2003]. Poleward boundary intensifications [e.g, *Zesta et al.*, 2000] might be another manifestation of the ballooning process developing at the PSLI. Possible interpretation of these findings with the ballooning instability will be a subject for further examination.

[44] **Acknowledgments.** We would like to thank G. Parks for providing Polar UVI data and M. Brittnacher for producing the UVI image plots. We acknowledge support by the "Österreichischer Austauschdienst" under Project I.12/04. Additional support was provided by the Austrian "Fonds zur Förderung der wissenschaftlichen Forschung" under Project P17099-N08, the Division of Physical Sciences of the Russian Academy of Sciences (program DPS-16 "Plasma processes in the solar system"), and the Presidium of the Russian Academy of Sciences (program 16).

[45] Lou-Chuang Lee thanks the reviewers for their assistance in evaluating this paper.

References

Alfvén, H. (1981), *Cosmic Plasma*, Springer, New York.

Angelopoulos, V., W. Baumjohann, C. F. Kennel, F. V. Coroniti, M. G. Kivelson, R. Pellat, R. J. Walker, H. Luhr, and G. Paschmann (1992), Bursty bulk flows in the inner central plasma sheet, *J. Geophys. Res.*, *97*, 4027.

Chang, S.-W., et al. (1998), A comparison of a model for the theta aurora with observations from Polar Wind and SuperDARN, *J. Geophys. Res.*, *103*, 17,367.

Craven, J. D., L. A. Frank, C. T. Russell, E. J. Smith, and R. P. Lepping (1986), Global auroral responses to magnetospheric compressions by shocks in the solar wind: Two case studies, in *Solar Wind – Magnetosphere Coupling*, edited by Y. Kamide and J. A. Slavin, p. 367, Terra Sci., Tokyo.

Crooker, N. U. (1979), Dayside merging and cusp geometry, *J. Geophys. Res.*, *84*, 951.

Cumnock, J. A., J. R. Sharber, R. A. Heelis, L. G. Blomberg, G. A. Germany, J. F. Spann, and W. R. Coley (2002), Interplanetary magnetic field control of theta aurora development, *J. Geophys. Res.*, *107*(A7), 1108, doi:10.1029/2001JA009126.

Frank, L. A., and J. D. Craven (1988), Imaging results from Dynamics Explorer 1, *Rev. Geophys.*, *26*, 249.

Frank, L. A., J. D. Craven, J. L. Burch, and J. D. Winningham (1982), Polar view of the Earth's aurora with Dynamic Explorer, *Geophys. Res. Lett.*, *9*, 1001.

Frank, L. A., et al. (1986), The theta aurora, *J. Geophys. Res.*, *91*, 3177.

Glassmeier, K.-H. (1983), Reflection of MHD-waves in the PC4-5 period range at ionospheres with non-uniform conductivity distributions, *Geophys. Res. Lett.*, *10*, 678.

Golovchanskaya, I. V., and Y. P. Maltsev (2003), Interchange instability in the presence of the field-aligned current: Application to the auroral arc formation, *J. Geophys. Res.*, *108*(A3), 1106, doi:10.1029/2002JA009505.

Golovchanskaya, I. V., and Y. P. Maltsev (2005), On the identification of plasma sheet flapping waves observed by Cluster, *Geophys. Res. Lett.*, *32*, L02102, doi:10.1029/2004GL021552.

Hameiri, E., P. Laurence, and M. Mond (1991), The ballooning instability in space plasmas, *J. Geophys. Res.*, *96*, 1513.

Hoffman, R. A., R. A. Heals, and J. S. Preside (1985), A sun-aligned arc observed by DMSP and AE-C, *J. Geophys. Res.*, *90*, 9,697.

Huang, C. Y., L. A. Frank, W. K. Peterson, D. J. Williams, W. Lennartsson, D. G. Mitchell, R. C. Elphic, and C. T. Russell (1987), Filamentary structures in the magnetotail lobes, *J. Geophys. Res.*, *92*, 2349.

Huang, C. Y., J. D. Craven, and L. A. Frank (1989), Simultaneous observations of a theta aurora and associated magnetotail plasmas, *J. Geophys. Res.*, *94*, 10,137.

Ivanov, V. N., O. A. Pokhotelov, F. Z. Feigin, A. Roux, S. Perraut, and D. Lecaux (1992), Ballooning instability in the Earth's magnetosphere under non-uniform pressure and finite β (in Russian), *Geomagn. Aeron.*, *32*, 68.

Kullen, A. (2000), The connection between transpolar arcs and magnetotail rotation, *Geophys. Res. Lett.*, *27*, 73.

Kullen, A., and P. Janhunen (2004), Relation of polar auroral arcs to magnetotail twisting and IMF rotation: A systematic MHD simulation study, *Ann.Geophys.*, *22*, 951.

Kullen, A., M. Brittnacher, J. A. Cumnock, and L. G. Blomberg (2002), Solar wind dependence of the occurrence and motion of polar auroral arcs: A statistical study, *J. Geophys. Res.*, *107*(A11), 1362, doi:10.1029/2002JA009245.

Lakhina, G. S., E. Hameiri, and M. Mond (1990), Ballooning instability of the Earth's plasma sheet region in the presence of parallel flow, *J. Geophys. Res.*, *95*, 10,441.

Lassen, K. (1979), The quiet time pattern of auroral arcs as a consequence of magnetospheric convection, *Geophys. Res. Lett.*, *6*, 777.

Lee, D.-Y., and R. A. Wolf (1992), Is the Earth's magnetotail balloon unstable?, *J. Geophys. Res.*, *97*, 19,251.

Liu, W. (1996), Note on the interchange stability criterion, *J. Geophys. Res.*, *101*, 27,447.

Liu, W. (1997), Physics of the explosive growth phase: Ballooning instability revisited, *J. Geophys. Res.*, *102*, 4927.

Lyatsky, W. B., and Y. P. Maltsev (1984), On the formation of the auroral bulge (in Russian), *Geomagn. Aeron.*, *24*, 89.

Makita, K., C.-I. Meng, and S.-I. Akasofu (1985), Temporal and spatial variations of the polar cap dimension inferred from the precipitation boundaries, *J. Geophys. Res.*, *90*, 2744.

Maltsev, Y. P. (1977), Boundary condition for Alfvén waves on the ionosphere (in Russian), *Geomagn. Aeron.*, *17*, 1008.

McEwen, D. J., and Y. Zhang (2000), A continuous view of the dawn-dusk polar cap, *Geophys. Res. Lett.*, *27*, 477.

Miura, A., S. Ohtani, and T. Tamao (1989), Ballooning instability and structure of diamagnetic hydromagnetic waves in a model magnetosphere, *J. Geophys. Res.*, *94*, 15,231.

Newell, P. T., D. Xu, C.-I. Meng, and M. G. Kivelson (1997), Dynamical polar cap: A unifying approach, *J. Geophys. Res.*, *102*, 127.

Ohtani, S., and T. Tamao (1993), Does the ballooning instability trigger substorms in the near-Earth magnetotail?, *J. Geophys. Res.*, *98*, 19,369.
Petrukovich, A. A., W. Baumjohann, R. Nakamura, A. Balogh, T. Mukai, K.-H. Glassmeier, H. Reme, and B. Klecker (2003), Plasma sheet structure during strongly northward IMF, *J. Geophys. Res.*, *108*(A6), 1258, doi:10.1029/2002JA009738.
Pontius, D. H., and T. W. Hill (1989), Rotation driven plasma transport: The coupling of macroscopic motion and microdiffusion, *J. Geophys. Res.*, *94*, 15,041.
Pontius, D. H., and R. A. Wolf (1990), Transient flux tubes in the terrestrial magnetosphere, *Geophys. Res. Lett.*, *17*, 49.
Rezhenov, B. V. (1995), A possible mechanism for theta aurora formation, *Ann. Geophys.*, *13*, 698.
Roux, A., S. Perraut, P. Roberts, A. Morane, A. Pedersen, A. Korth, G. Kremser, B. Aparicio, D. Rodgers, and R. Pellinen (1991), Plasma sheet instability related to the westward traveling surge, *J. Geophys. Res.*, *96*, 17,697.
Sergeev, V. A., et al. (2000), Multi-spacecraft observation of a narrow transient plasma jet in the Earth's plasma sheet, *Geophys. Res. Lett.*, *27*, 851.
Song, P., D. L. DeZeeuw, T. I. Gombosi, C. P. T. Groth, and K. G. Powell (1999), A numerical study of solar wind-magnetosphere interaction for northward interplanetary magnetic field, *J. Geophys. Res.*, *104*, 28,361.
Tsyganenko, N. A. (1995), Modeling the Earth's magnetospheric magnetic field confined with a realistic magnetopause, *J. Geophys. Res.*, *100*, 5599.
Valladares, C. E., and H. C. Carlson (1991), The electrodynamic, thermal, and energetic character of intense sun-aligned arcs in the polar cap, *J. Geophys. Res.*, *96*, 1379.
Valladares, C. E., H. C. Carlson Jr., and K. Fukui (1994), Interplanetary magnetic field dependency of stable sun-aligned polar cap arcs, *J. Geophys. Res.*, *99*, 6247.
Weimer, D. R. (1995), Models of high-latitude electric potential derived with a least error fit of spherical harmonic coefficients, *J. Geophys. Res.*, *100*, 19,595.
Zesta, E., L. R. Lyons, and E. Donovan (2000), The auroral signature of Earthward flow bursts observed in the magnetotail, *Geophys. Res. Lett.*, *27*, 3241.

H. Biernat, Space Research Institute, Austrian Academy of Sciences, Schmiedlstrasse 6, A-8042 Graz, Austria. (helfried.biernat@oeaw.ac.at)
I. V. Golovchanskaya, Polar Geophysical Institute, Apatity, Murmansk region, 184209, Russia. (golovchanskaya@pgi.kolasc.net.ru)
A. Kullen, Swedish Institute of Space Physics, Box 537, SE-751 21 Uppsala, Sweden. (anita.kullen@irfu.se)